iScience

CellPress
OPEN ACCESS

Article

Characterization and mechanism investigation of salt-activated methionine sulfoxide reductase A from halophiles

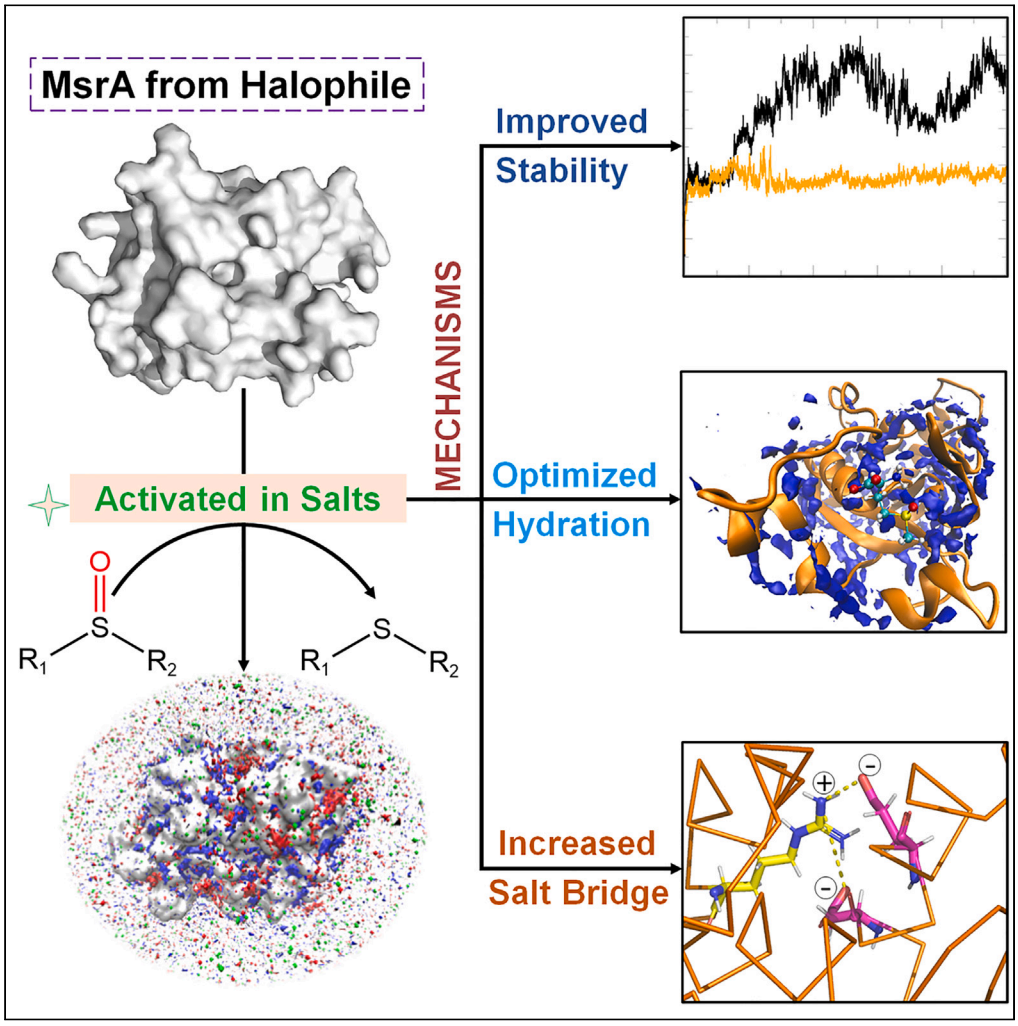

Shihuan Zhou, Bochen Pan, Xiaoxue Kuang, ..., Xianlin Xu, Xiaoling Cheng, Jiawei Yang

xiaoling_cheng@qq.com (X.C.)
yangjw@zmu.edu.cn (J.Y.)

Highlights

MsrA activity from halophiles is induced by salts

Salt ions stabilize MsrA structure and enhance substrate affinity

Salt bridges triggered by Arg168 are crucial and its mutation disrupts salt activation

Zhou et al., iScience 27, 110806
September 20, 2024
https://doi.org/10.1016/j.isci.2024.110806

iScience

CellPress
OPEN ACCESS

Article

Characterization and mechanism investigation of salt-activated methionine sulfoxide reductase A from halophiles

Shihuan Zhou,[1,3] Bochen Pan,[1,3] Xiaoxue Kuang,[1,3] Shuhong Chen,[1] Lianghui Liu,[1] Yawen Song,[1] Yuyan Zhao,[1] Xianlin Xu,[1] Xiaoling Cheng,[2,*] and Jiawei Yang[1,4,*]

SUMMARY

Halophiles, thriving in harsh saline environments, capture scientific interest due to their remarkable ability to prosper under extreme salinity. This study unveils the distinct salt-induced activation of methionine sulfoxide reductases (MsrA) from *Halobacterium hubeiense*, showcasing a significant enhancement in enzymatic activity across various salt concentrations ranging from 0.5 to 3.5 M. This contrasts sharply with the activity profiles of non-halophilic counterparts. Through comprehensive molecular dynamics simulations, we demonstrate that salt ions stabilize and compact the enzyme's structure, notably enhancing its substrate affinity. Mutagenesis analysis further confirms the essential role of salt bridges formed by the basic Arg168 residue in salt-induced activation. Mutating Arg168 to an acidic or neutral residue disrupts salt-induced activation, substantially reducing the enzyme activity under salt conditions. Our research provides evidence of salt-activated MsrA activity in halophiles, elucidating the molecular basis of halophilic enzyme activity in response to salts.

INTRODUCTION

Extremophiles are microorganisms that thrive in extreme environments, such as extreme temperatures, high radiation, acidic or alkaline environments, and even the depths of the ocean floor.[1] Their unique biochemical and physiological adaptations have garnered significant scientific interest due to their potential applications in various fields, including biotechnology, astrobiology, and environmental science.[2–7] Halophiles constitute a fascinating group of extremophiles that thrive in saline or hypersaline environments.[4,8] According to the optimum salt concentration required for their growth, halophiles can be categorized as slight halophiles (0.2–0.5 M salt), moderate halophiles (0.5–2.5 M salt), and extreme halophiles (2.5–5.2 M salt).[9] Owing to their distinctive structural and physicochemical characteristics, halophiles have garnered significant attention in biotechnological applications, such as high-salt fermentation, high-salt wastewater treatment, biofuel production, and the exploration of enzymes derived from halophilic microorganisms.[4,9–12] Furthermore, understanding the mechanisms by which these microorganisms adapt to high-salt environments has also been a fascinating pursuit for scientists.[8,13–17]

Halophiles have developed several remarkable adaptations to cope with high salinity, including the "salt-in strategy" involving potassium ion accumulation, the production of "halophilic proteins" to repel sodium ions, and the synthesis of "osmoprotectants" like betaine and trehalose to protect cellular structures from osmotic stress.[17,18] These strategies collectively enable their survival in extreme saline environments. Usually, high salt concentration environments can denature and destabilize proteins, which may inhibit the catalytic activity and impair the structural integrity of enzymes.[19] However, halophilic proteins generally remain stable and functional under high salt concentrations.[20] These proteins feature negatively charged surfaces, contrasting with typical proteins with neutral or slightly positive charges, which allow them to repel positively charged ions.[21–23] They also exhibit a more flexible structure, promoting efficient interaction with water molecules to counteract dehydration caused by high salt concentrations.[24] Many halophilic proteins display enhanced thermostability, which is crucial in high-temperature, high-salt conditions.[20] Additionally, some possess specialized salt-binding pockets, aiding stability and functionality in saline environments.[25,26] A deeper understanding of how halophilic proteins maintain their structure and prevent aggregation in challenging environments could offer valuable insights for the field of biotechnology.

Methionine sulfoxide reductases (Msr) are a family of enzymes responsible for catalyzing the reduction of methionine sulfoxide (Met-O) back to its biologically active methionine (Met) form.[27] In living cells, Met is relatively easily oxidized to sulfoxide under mild conditions.[28] For many proteins, oxidation of Met residues to the Met-O results in the loss of their biological properties.[29] Thus, Msr enzymes play a crucial role in cellular antioxidant defense mechanisms and the maintenance of protein functionality.[30] On the other hand, oxidation of Met creates a

[1]Department of Biochemistry, School of Preclinical Medicine, Zunyi Medical University, Zunyi 563000, Guizhou, China
[2]Department of Cell Biology, School of Preclinical Medicine, Zunyi Medical University, Zunyi 563000, Guizhou, China
[3]These authors contributed equally
[4]Lead contact
*Correspondence: xiaoling_cheng@qq.com (X.C.), yangjw@zmu.edu.cn (J.Y.)
https://doi.org/10.1016/j.isci.2024.110806

chiral center at the sulfur atom, making the produced Met-O a mixture of *S* and *R* enantiomers.[31] Therefore, different types of reductases, like MsrA and MsrB, are active on each enantiomer of Met-O due to their enantioselectivity.[27] The excellent enantioselectivity of different types of Msr enzymes makes them outstanding biocatalysts for the green synthesis of enantiopure sulfoxide compounds in the field of biotechnology.[32–41] As an outstanding protector of cells from the harmful effects of oxidative stress,[42] the Msr enzymes probably play pivotal roles in the survival of halophilic cells in high-salt-stress environments. Recently, it has been reported that the MsrA from *Haloferax volcanii* exhibits ubiquitin-like (Ubl) protein modification activity, in addition to its well-known stereospecific reduction of Met-O. This discovery provides insights into oxidative stress responses that can induce Ubl modification within a cell.[43] Nevertheless, the enzymatic characteristics and mechanisms of Msr in halophilic microorganisms in response to salts remain unexplored. In this study, we revealed that the activity of the MsrA enzyme from halophile *Halobacterium hubeiense* strain JI20-1 (named *Hh*MsrA) was activated by high salt concentrations. We further elucidated the related mechanisms using molecular dynamics (MD) simulation and mutagenesis analysis, providing perspectives on understanding the mechanisms underlying salt ion activation in halophilic proteins.

RESULTS AND DISCUSSION

Recombinant expression and activity characterization of MsrA from halophile *H. hubeiense* strain JI20-1

The DNA fragment of the *Hh*MsrA gene (gene ID: 26659341) was first synthesized based on the GenBank database and cloned into the expression plasmid. The results of SDS-PAGE analysis confirmed that the target protein was effectively expressed in a soluble form after induction by isopropyl β-D-1-thiogalactopyranoside (Figure S1). After purification using the His-tag, enzymatic studies revealed that *Hh*MsrA exhibited minimal activity when Met-O was used as the substrate (Figure 1A). Considering the survival of *Halobacterium* genus in high-salt environments,[44] we hypothesized that the activity of *Hh*MsrA could be activated by high-salt conditions. Thus, KCl was added to the reaction at a final concentration of 1.5 M. The results showed a significant improvement in catalytic activity, with the specific activity reaching 81.2 ± 5.3 U/g (Figure 1A), strongly suggesting that high-salt ions were essential for the activity of MsrA in this haloarchaeon. In contrast, the activity of MsrA from a non-halophilic *Pseudomonas monteilii* strain (*pm*MsrA), which we isolated previously,[32] was inhibited with increasing salt concentrations (Figure S2). These data demonstrate the activation of MsrA in halophiles by high concentrations of salt ions.

Afterward, we evaluated temperature and pH characteristics of *Hh*MsrA in the presence of 1.5 M KCl. Initially, the relative activities of *Hh*MsrA over a temperature range of 20°C–50°C were determined. The enzyme exhibited its peak activity at 40°C, retaining over 80% of its activities within the 35°C–45°C range (Figure 1B). Previous studies have shown that enzymes from halophiles exhibit higher optimal reaction temperature and greater thermal stability.[45,46] Our research is consistent with these studies, as the optimal reaction temperature of 40°C is higher than that of MsrA homologs from non-halophilic cells, which are usually around 30°C and sensitive to temperature.[33,37,47] The enzyme's exceptional temperature adaptability suggests potential advantages in the field of industrial biotechnology, where thermostability is deemed a critical parameter for assessing the feasibility of enzymes for industrial application.[48] Subsequent investigations focused on the impact of pH on the activity of *Hh*MsrA, spanning pH values from 4.0 to 11.0. The results indicated that the enzyme showed basophilic properties with the highest activity at pH 10.0, retaining over 90% of its activities between pH 10.0 and 11.0 (Figure 1C). However, the activity of *Hh*MsrA was significantly reduced when the reaction pH was lower than 8.0. Based on these results, 40°C and pH 10.0 were designated as the reaction conditions for subsequent studies.

Effects of various salts on *Hh*MsrA activity

To further assess the impact of salts on the *Hh*MsrA activity, the specific activities of *Hh*MsrA were determined under various monovalent and bivalent neutral salts, including KCl, NaCl, $CaCl_2$, K_2SO_4, and Na_2SO_4. The results revealed that all tested salts significantly activated the enzyme *Hh*MsrA. Among them, KCl and NaCl exhibited the strongest activation, with similar profiles (Figures 2A and 2B). Enzyme activity was observed at concentrations higher than 0.5 M of KCl or NaCl and elevated with increasing salt concentrations. The activation effects of both KCl and NaCl were most pronounced between 0 and 1.0 M, and the peak activity was observed at the highest concentration of 3.5 M for both salts, achieving 95.1 ± 6.7 U/g and 78.6 ± 9.3 U/g, respectively. In addition, specific activities were slightly higher under KCl than under NaCl at most concentrations. While a previous report suggested that *H. hubeiense* JI20-1 required NaCl for growth,[44] our findings indicate that the activating effect of K^+ ions was more pronounced than that of Na^+ ions on the *Hh*MsrA enzyme. Regarding $CaCl_2$, the activation effect was similar to that of NaCl, but the salt concentration required for activation was much lower. The enzyme exhibited peak activity under 0.5 M $CaCl_2$, achieving 78.8 ± 3.4 U/g (Figure 2C), indicating that the activation effect of Ca^{2+} ions was much stronger than that of Na^+ ions. However, unlike KCl and NaCl, the activities of *Hh*MsrA decreased at concentrations higher than 0.5 M $CaCl_2$ and were completely inhibited at 3.0 M, indicating that the high concentrations of Ca^{2+} ions could inhibit *Hh*MsrA activity.

For the two sulfates, K_2SO_4 and Na_2SO_4, their activation effects were much weaker compared to their chlorides (Figures 2D and 2E). Peak activities were observed at 0.4 M K_2SO_4 and 1.2 M Na_2SO_4, achieving only 25.6 ± 5.6 U/g and 18.0 ± 5.5 U/g, respectively. Unlike their chloride counterparts, the high concentrations of K_2SO_4 and Na_2SO_4 inhibited enzyme activities. To test whether these inhibitions are reversible or not, we first treated the enzyme in the presence of 2.0 M of Na_2SO_4 for 45 min, and then measured its activity under 1.0 and 2.0 M KCl conditions. The results showed that only 36% of residual activities were detected in both conditions (Figure S3), suggesting that high concentration of sulfates can result in irreversible inhibition of the enzyme. This irreversible inhibition suggests that sulfate ions may cause permanent structural changes and denaturation of the enzyme, as indicated by the observed protein precipitation after treatment.

Taken together, the activity of *Hh*MsrA was activated by all test salts, with chlorides showing much stronger effects than the corresponding sulfates. Both monovalent Na^+ and K^+ ions, as well as bivalent Ca^{2+} ions, could activate the enzyme *Hh*MsrA, with monovalent Na^+ and K^+ ions

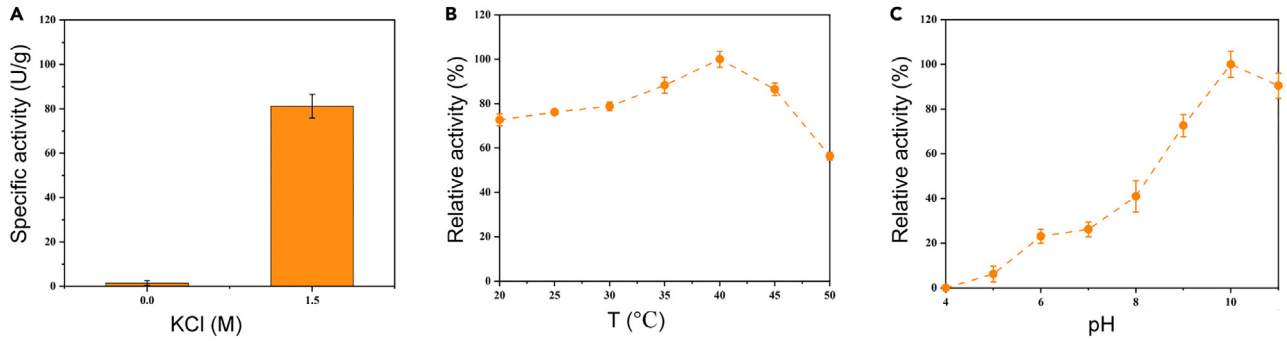

Figure 1. Characterization of the enzymatic properties of *Hh*MsrA

(A) Specific activity analysis of *Hh*MsrA with 0 and 1.5 M KCl.

(B and C) Temperature and pH profiles of *Hh*MsrA. The *Hh*MsrA activities were assayed using the DTT-DTNB coupled colorimetric method. Each reaction was performed in the presence of 3 μM of pure enzyme, 3 mM of Met-O, and 1 mM of DTT for 45 min. Each value represents the mean ± SD of three independent experiments.

exhibiting a greater tolerance under higher concentrations in activating the enzyme. Considering the survival of *H. hubeiense* under high-salt conditions,[44] the activation of MsrA by various salts may potentially contribute to protecting these cells from oxidative stress in high-salt conditions. Numerous reports have illustrated that halophiles developed several remarkable adaptations to cope with high salinity.[18,20,25] This study implies that the MsrA-mediated antioxidation system could also play essential roles in the survival of these halophiles under high-salt conditions, providing insights into the mechanisms by which halophilic microorganisms survive in such environments.

Substrate specificity analysis of *Hh*MsrA for various sulfoxide substrates

Previous studies have shown that MsrA homologs from non-halophilic species exhibited excellent activities toward a series of sulfoxide substrates.[33,38,39] To further understand the substrate specificity of this *Hh*MsrA enzyme, various aryl alkyl sulfoxides, dialkyl sulfoxides, and thioalkyl sulfoxides (Figure S4) were used as substrates to test its activity under the condition of 3.5 M KCl. The results revealed that the enzyme was active on all substrates containing a methyl/ethyl moiety on the sulfinyl group, with specific activities ranging from 24.4 ± 7.8 U/g to 115.8 ± 6.7 U/g, depending on their structures (Figure 3). As observed, *Hh*MsrA exhibits maximal activity against 1-(methylsulfinyl) propane rather than the natural substrate Met-O and also shows higher activity against 1-(methylsulfinyl)pentane and 1-(methylsulfinyl) decane compared to Met-O. This substrate preference may be attributed to the specific structural features of *Hh*MsrA's active site, which likely favors the binding of these substrates due to better steric and hydrophobic interactions. The structural configuration of these substrates may align more effectively with the enzyme's active site, enhancing catalytic efficiency. Further structural studies could provide more insights into these interactions. However, for substrates in which the methyl/ethyl moiety was substituted by a larger propyl/butyl moiety, such as (propylsulfinyl)benzene, (isopropylsulfinyl)benzene, and (butylsulfinyl)benzene, *Hh*MsrA was inactive. These substrate profiles were also similar to those of homologs from non-halophilic species.[33,38,39]

Mechanism investigation of salt activation of *Hh*MsrA

To elucidate the mechanism underlying the activation of *Hh*MsrA by salts, 100 ns MD simulations of *Hh*MsrA-substrate (Met-*S*-O) complexes were performed with and without the presence of KCl (1.0 M). The enzyme's stability was compared by analyzing several parameters, including root-mean-square deviation (RMSD),[49] solvent-accessible surface area (SASA),[50] and radius of gyration (Rg).[51] As illustrated in Figure 4A, the RMSD values of the enzyme displayed significant fluctuations after 20 ns in the absence of KCl. In contrast, in the presence of KCl, the system remained stable throughout the simulation, with an average RMSD value of 0.263 nm, significantly lower than that in the absence of KCl (0.459 nm). As a commonly used indicator for assessing protein structure stability throughout the simulation,[49] the RMSD measurement indicates that the presence of KCl enhances the stability of *Hh*MsrA. Furthermore, the enzyme exhibited lower SASA and Rg values in the presence of KCl, indicating a more compact structure (Figures 4B and 4C). Collectively, the data obtained through MD simulations indicate that the presence of KCl enhances the stability of the enzyme during catalytic processes.

To further validate these data, the half-life of *Hh*MsrA at 30°C was determined in both the absence and presence of KCl. As illustrated in Figure 4D, the half-life of *Hh*MsrA was only 24.3 h without KCl. However, in the presence of KCl, this metric extended to 133.1 h, approximately 5 times longer than without salt. Moreover, we analyzed the pH-stability profile of the enzyme in the presence and the absence of KCl to further validate the stability. We analyzed the activity of *Hh*MsrA pre-treated at pH 5.0, 7.0, and 11.0 with or without KCl, for durations of 2 and 10 h. The data showed that pre-treatment with salts under unfavorable pH conditions, such as pH 5.0, could greatly reduce the enzyme's activity (Figure S5). However, the presence of salt was highly effective in maintaining the enzyme's activity. For instance, after treatment for 10 h at pH 5.0, the residual activities of *Hh*MsrA were 30.2% and 80.4% with and without KCl, respectively (Figure S5). These experiments validated the MD results and strongly verified that the presence of salts greatly enhances the enzyme's stability.

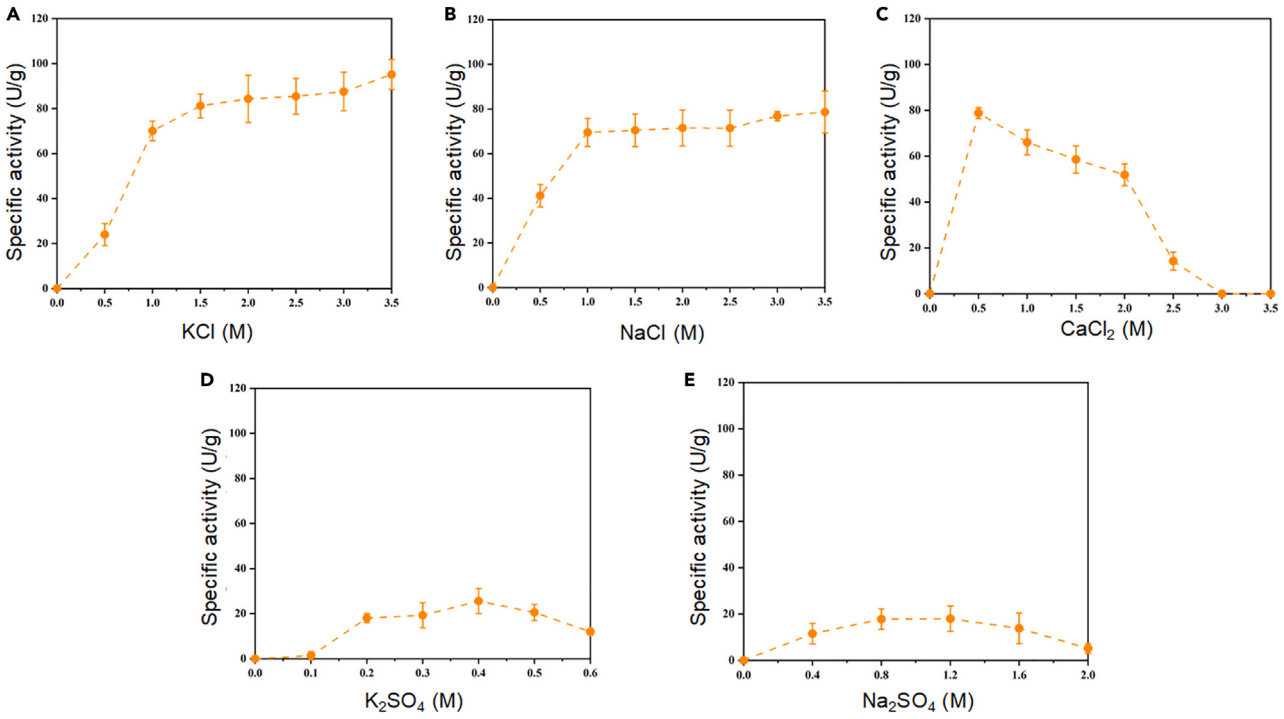

Figure 2. Effects of various salts on *Hh*MsrA's activity

The activity of *Hh*MsrA was assessed in the presence of different salts: KCl (A), NaCl (B), $CaCl_2$ (C), K_2SO_4 (D), and Na_2SO_4 (E). Specific activities were assayed using the DTT-DTNB coupled colorimetric method, consistent with those in Figure 1, using Met-O as the substrates under conditions of 40°C and pH 10.0. Each value represents the mean ± SD of three independent experiments.

Previous studies on the crystal structure of halophilic 2Fe-2S ferredoxin reveal that haloadaptation involves an enhanced water-binding capacity.[52] Thus, the effect of KCl on the stability of the hydration layer around *Hh*MsrA was investigated. We employed the spatial distribution function to visualize the distribution of the water molecules and ions around *Hh*MsrA. As depicted in Figures 4E and 4F, the water molecules and ions (mainly K^+) were distributed on the surface of the protein, with an increased number of water molecules in certain regions following the addition of KCl. Statistical analysis of the number of water molecules within the active site revealed that the addition of KCl increased the number of water molecules within the active pocket and reduced their fluctuations in this region (Figure 4G). These findings indicate that the KCl improves the distribution and quantity of water molecules of the enzyme, consequently optimizing its conformation and probably enhancing the enzyme-substrate binding.[53,54] Thus, we determined the kinetic parameters of *Hh*MsrA under low (0.8 M) and high salts (1.5 M). The K_m and K_{cat} of the enzyme under low salt were 4.301 mM and 0.133 s^{-1}, respectively (Table 1). Notably, with the increase in salt concentration, the K_m was reduced to 0.503 mM, indicating that the high salt concentration greatly enhanced the enzyme's affinity for the substrate. Combining the results of MD simulations, stability experiments, and enzymatic kinetics experiments, these findings suggest that the addition of salt enhances the structural stability of *Hh*MsrA by reducing fluctuations and compacting the structure and strengthens the stability of the hydration layer. These combined factors contribute to the improved stability of the enzyme in salt-rich environments, consequently enhancing the enzyme-substrate affinity, which positively influences its activity.

Investigation of salt bridges regarding the activation of *Hh*MsrA by salts

Salt bridges are pivotal for the structural stability of halophilic proteins, particularly in high-salt environments.[45,55,56] They enhance internal electrostatic interactions within the protein, thereby preserving its three-dimensional structure and ultimately bolstering its stability. For instance, comparing the three-dimensional structures of halophilic malate dehydrogenase with its non-halophilic counterparts reveals a greater presence of salt bridges in halophilic malate dehydrogenase.[21] We thus analyzed changes in salt bridges during the 100 ns MD simulations with or without KCl. Our analysis revealed that the presence of KCl leads to an increase in the total number and duration within *Hh*MsrA and decrease in their fluctuations (Figure 5A). These data indicate that the addition of KCl could potentially enhance the enzyme's interaction network favorably. Notably, we observed substantial variations in salt bridges triggered by the residue Arg168, which is located on the surface of the enzyme, far from the active center (Figure 5B). In the presence of KCl, this residue formed salt bridges with Asp69 and Glu72 with durations of 46.44 and 29.55 ns, respectively, during the 100 ns simulation (Figure 5C). However, in the absence of KCl, the enzyme underwent certain conformational changes, resulting in the reorientation of the positively charged side chain of Arg168 away from the acidic

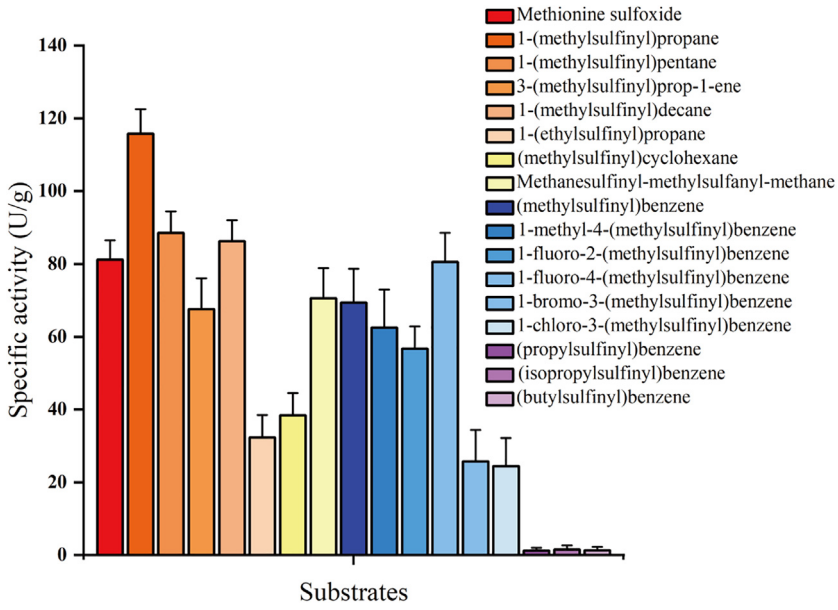

Figure 3. Specific activity analysis of *Hh*MsrA toward a series of sulfoxide substrates

The reaction conditions are consistent with those in Figure 2 in the presence of 3.5 M KCl. Each value represents the mean ± SD of three independent experiments.

amino acids Asp69 and Glu72. This change led to the formation of substituted salt bridges between Arg168 and Asp120, and Arg168 and Glu72, with significantly shorter durations, lasting only 29.43 and 15.93 ns, respectively (Figure 5D).

To further verify the essential role of the salt bridge formed by Arg168, mutagenesis analysis was conducted for this critical amino acid residue. We introduced mutations at this site, substituting the basic Arg168 with various other amino acids, including the basic Lys, acidic Glu, hydrophobic Ala and Pro, and aromatic Phe. All resulting variants were successfully expressed in soluble form and purified from *E. coli* (Figure S1). As shown in Figure 6A, when this Arg residue was replaced by another basic Lys (*Hh*MsrA-R168K), the KCl profiles at all concentrations remained virtually unchanged, indicating that substituting amino acids with similar properties did not alter *Hh*MsrA's salt activation. Variants including *Hh*MsrA-R168F, *Hh*MsrA-R168A, *Hh*MsrA-R168E, and *Hh*MsrA-R168P exhibited minimal activities at 0.5 M of KCl. Even under optimal salt concentrations, their activities were less than half of those observed for *Hh*MsrA-wild type (WT) and *Hh*MsrA-R168K. Notably, the variant *Hh*MsrA-R168P exhibited a peak activity of only 24.3 ± 7.4 U/g, which is a quarter of that of *Hh*MsrA-WT. These findings underscore the critical role of the basic amino acid at position 168 in maintaining enzyme stability and facilitating salt activation.

Variants *Hh*MsrA-R168K and *Hh*MsrA-R168P were then selected for MD simulations to assess their performances in the presence of 1.0 M KCl. As shown in Figures 6B–6D, the values of RMSD, SASA, and Rg values between enzymes *Hh*MsrA-WT and *Hh*MsrA-R168K exhibit relatively minor differences. However, for the variant *Hh*MsrA-R168P, all these parameters were unfavorable compared to *Hh*MsrA-WT and *Hh*MsrA-R168K. These results suggest that substituting Arg168 with an amino acid sharing similar properties minimally affects enzyme stability, whereas substitution with other types of amino acids substantially weakens it. The half-life of *Hh*MsrA-R168K variant at 30°C was determined, and the results were consistent with those of the WT enzyme (Figure S6). These results further confirmed that this mutagenesis did not alter the enzyme's stability. However, substitution with other types of amino acids significantly weakened the salt activation effects. Furthermore, the salt bridge analysis revealed that mutating Arg168 to Pro significantly reduced both the total number and duration of salt bridges compared to those observed in the *Hh*MsrA-WT and *Hh*MsrA-R168K (Figure 6E). Notably, in the *Hh*MsrA-R168K variant, although the salt bridge between Arg168 and Asp69 in *Hh*MsrA-WT disappeared, the salt bridge between Arg168 and Glu72 shortened the distances between certain nearby amino acids. This, in turn, led to the formation of two new salt bridges between Lys166 and both Glu72 and Asp69, maintaining the stability of its spatial conformation (Figure 6F). Conversely, within the *Hh*MsrA-R168P variant, the mutated Pro was far from the corresponding amino acids and failed to form any salt bridges with other residues, resulting in significant spatial conformation changes compared to the *Hh*MsrA-WT enzyme (Figure 6F).

Moreover, the kinetic parameters of *Hh*MsrA-R168K and *Hh*MsrA-R168P under high salts (1.5 M) were compared. The results showed that the K_m and K_{cat} values of *Hh*MsrA-R168K were quite consistent with those of the WT enzyme (Table 1), indicating this mutagenesis did not cause significant changes to the enzymatic properties. However, the K_m of *Hh*MsrA-R168P was 1.141 mM, much higher than those of WT and *Hh*MsrA-R168K, suggesting that the mutagenesis of basic Arg to hydrophobic Pro leads to a lower substrate affinity. In addition, the K_{cat} value of *Hh*MsrA-R168P was also slightly lower, indicating this mutagenesis also resulted in a decrease in catalytic rate. All these data suggest that salt bridges formed by the basic residue at position 168 play crucial roles in the enzyme's response to salts, enhancing its stability and ultimately activating its catalytic activity.

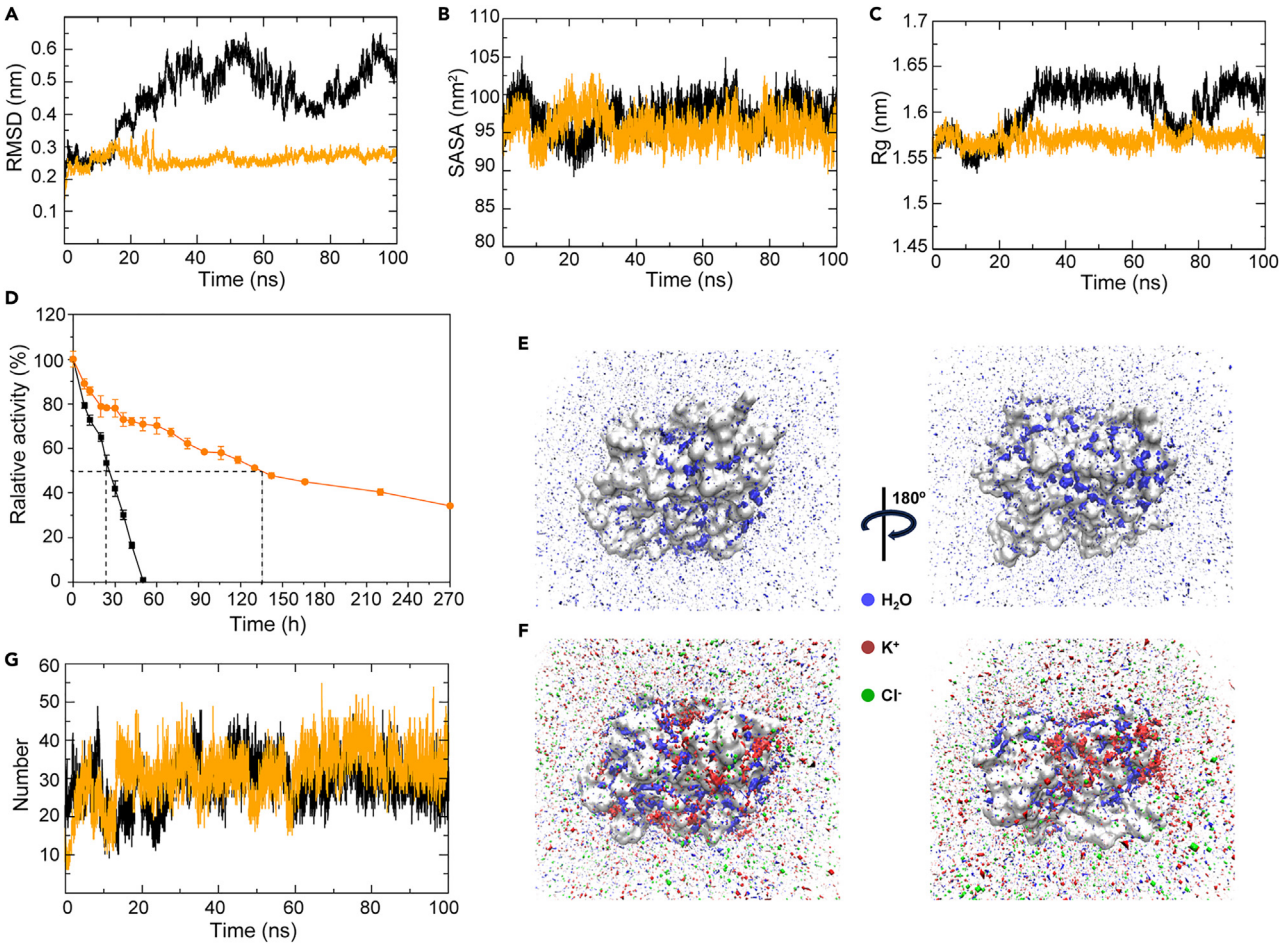

Figure 4. MD simulation and stability analysis of *Hh*MsrA under conditions with or without KCl

Met-*S*-O was used as substrate for the simulation. The black and orange lines represent data obtained in the absence and presence of KCl, respectively.

(A) Root-mean-square deviation (RMSD) for the main chain atoms.

(B) Solvent-accessible surface area (SASA).

(C) Radius of gyration (Rg).

(D) Half-life analysis of *Hh*MsrA in the absence and presence of KCl, each value represents the mean ± SD of three independent experiments.

(E and F) Spatial distribution of water molecules, K^+, and Cl^- ions on the surface of the *Hh*MsrA in the absence (E) and presence (F) of KCl. The protein surface, water molecules, K^+ ions, and Cl^- ions are shown in gray, blue, red, and green, respectively.

(G) Number of water molecules in the active site.

In summary, our study presents evidence that the activity of MsrA from halophile is activated by various salts, offering insights into the antioxidation roles contributing to the survival of halophiles in high-salt environments. Molecular docking, MD simulations, stability, and kinetic assays revealed that the presence of salts enhances the structural stability of the enzyme, resulting in improved enzyme-substrate binding and catalytic efficiency. Furthermore, site-directed mutagenesis experiments demonstrated the essential role of specific amino acid residues, particularly Arg168, in mediating the enzyme's response to salts. Substitution of Arg168 with different amino acids significantly impacted enzyme stability and salt activation. These findings deepen the understanding of the molecular basis of salt adaptation in halophilic microorganisms and provide insights for the design of enzymes with enhanced stability and activity under extreme environmental conditions.

Limitations of the study

This study proposes that the salt bridge is an essential factor for the MsrA enzyme from halophiles in responding to high salinity, as evidenced by MD simulations and mutagenesis analysis. Further analysis of the crystal structure is required to confirm the significance of this factor. Moreover, since all *Hh*MsrA variants retained a certain level of activity, future studies will explore other contributing factors influencing the enzyme's response to high salinity.

Table 1. Kinetic parameters of *Hh*MsrA and variants

Entry	Enzyme	KCl (M)	K_m (mM)	K_{cat} (s^{-1})	K_{cat}/K_m ($s^{-1} \cdot mM^{-1}$)
1	*Hh*MsrA-WT	0.8	4.301	0.133	0.031
2	*Hh*MsrA-WT	1.5	0.503	0.169	0.336
3	*Hh*MsrA-R168K	1.5	0.579	0.173	0.299
4	*Hh*MsrA-R168P	1.5	1.411	0.110	0.078

RESOURCE AVAILABILITY

Lead contact

Further information and requests for resources and reagents should be directed to and will be fulfilled by the lead contact, Jiawei Yang (yangjw@zmu.edu.cn).

Materials availability

This study did not generate new unique reagents.

Data and code availability

All data reported in this paper will be shared by the lead contact upon request.

This paper does not report original code.

All other requests: Any additional information required to reanalyze the data reported will be shared by the lead contact upon request.

ACKNOWLEDGMENTS

This work was supported by Guizhou Science and Technology Department (no. QKHJC-ZK-2023YB521 and QKHJC-ZK-2021-ZD028), National Natural Science Foundation of China (no. 32260228 and 31960202), and the Zunyi Science and Technology Department (ZSKH-HZ2023-193 and QKPTRC-2021-1350-029).

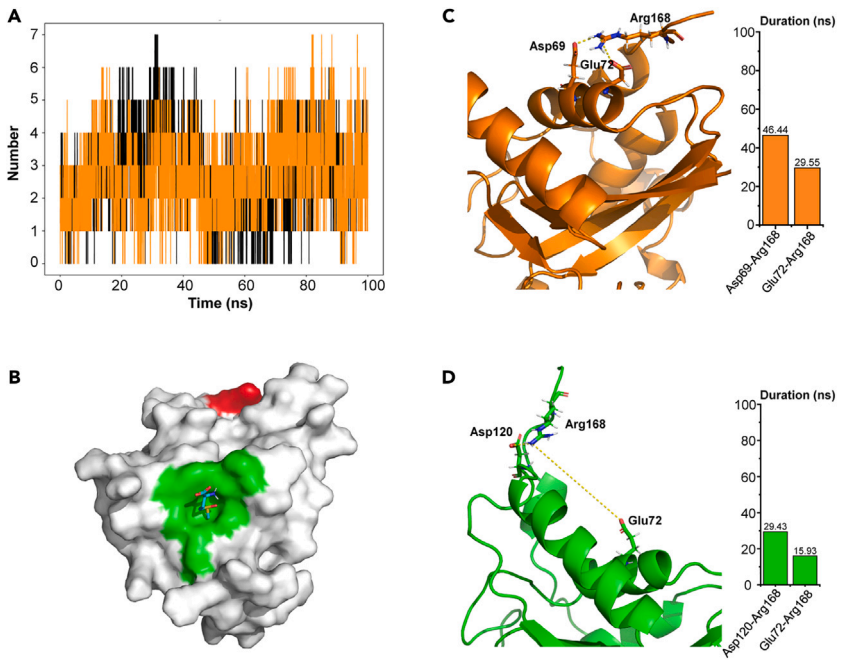

Figure 5. Analysis of salt bridge formations in *Hh*MsrA during a 100 ns MD simulation

(A) Number of total salt bridges within *Hh*MsrA during simulation. The black and orange lines represent data obtained in the absence and presence of KCl, respectively.

(B) 3D model of *Hh*MsrA docking with substrate Met-*S*-O. The green and red regions represent the active center and Arg168, respectively. The sticks represent the substrate.

(C and D) Structure and duration analysis of residue Arg168 salt bridge in the presence (C) and absence of KCl (D).

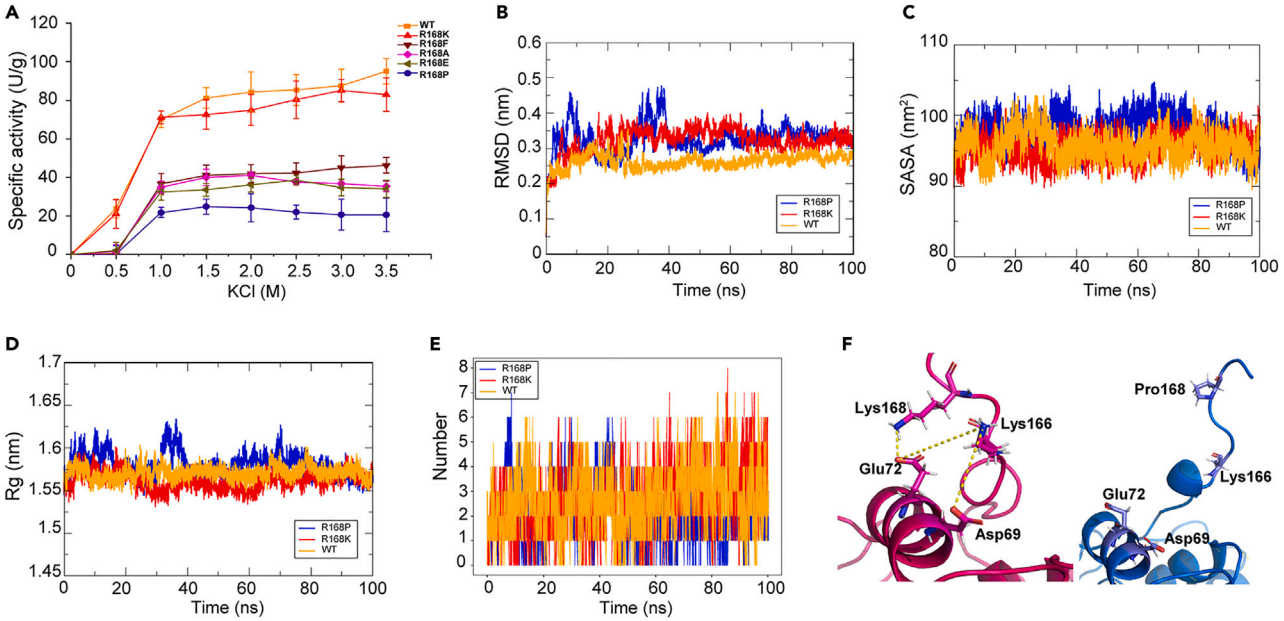

Figure 6. Mutagenesis analysis of key amino acid residue within *Hh*MsrA

(A) Specific activities of *Hh*MsrA-WT and its variants under various concentrations of KCl, each value represents the mean ± SD of three independent experiments.

(B–D) RMSD (B), SASA (C), and Rg (D) comparisons between *Hh*MsrA-WT and the variants *Hh*MsrA-R168K and *Hh*MsrA-R168P.

(E) Total number of salt bridges within variants *Hh*MsrA-R168K and *Hh*MsrA-R168P during simulation.

(F) Structure analysis of salt bridge involving key residue 168 within variants *Hh*MsrA-R168K (red) and *Hh*MsrA-R168P (blue).

AUTHOR CONTRIBUTIONS

Conceptualization, X.C. and J.Y.; methodology, B.P., S.C., and X.X.; investigation, S.Z., B.P., X.K., and Y.Z.; software, B.P., Y.S., and L.L.; writing – original draft, S.Z., B.P., and X.K.; writing – review and editing, X.C. and J.Y.; funding acquisition, X.C. and J.Y.; resources, J.Y.; supervision, X.C. and J.Y.

DECLARATION OF INTERESTS

The authors declare no competing interests.

STAR★METHODS

Detailed methods are provided in the online version of this paper and include the following:

- KEY RESOURCES TABLE
- EXPERIMENTAL MODEL AND STUDY PARTICIPANT DETAILS
  - Microbe strains
- METHODS DETAILS
  - Recombinant expression and purification of *Hh*MsrA and variants
  - Enzyme activity assays
  - Half-life and pH stability analysis
  - Kinetic parameters determination
  - Site-directed mutagenesis
  - Molecular docking and MD simulations
- QUANTIFICATION AND STATISTICAL ANALYSIS

SUPPLEMENTAL INFORMATION

Supplemental information can be found online at https://doi.org/10.1016/j.isci.2024.110806.

Received: March 4, 2024
Revised: July 23, 2024
Accepted: August 20, 2024
Published: August 23, 2024

REFERENCES

1. Dumorné, K., Córdova, D.C., Astorga-Eló, M., and Renganathan, P. (2017). Extremozymes: A Potential Source for Industrial Applications. J. Microbiol. Biotechnol. *27*, 649–659. https://doi.org/10.4014/jmb.1611.11006.
2. Shrestha, N., Chilkoor, G., Vemuri, B., Rathinam, N., Sani, R.K., and Gadhamshetty, V. (2018). Extremophiles for microbial-electrochemistry applications: A critical review. Bioresour. Technol. *255*, 318–330. https://doi.org/10.1016/j.biortech.2018.01.151.
3. Barnard, D., Casanueva, A., Tuffin, M., and Cowan, D. (2010). Extremophiles in biofuel synthesis. Environ. Technol. *31*, 871–888. https://doi.org/10.1080/09593331003710236.
4. Chettri, D., Verma, A.K., Sarkar, L., and Verma, A.K. (2021). Role of extremophiles and their extremozymes in biorefinery process of lignocellulose degradation. Extremophiles *25*, 203–219. https://doi.org/10.1007/s00792-021-01225-0.
5. Carré, L., Zaccai, G., Delfosse, X., Girard, E., and Franzetti, B. (2022). Relevance of Earth-Bound Extremophiles in the Search for Extraterrestrial Life. Astrobiology *22*, 322–367. https://doi.org/10.1089/ast.2021.0033.
6. Obulisamy, P.K., and Mehariya, S. (2021). Polyhydroxyalkanoates from extremophiles: A review. Bioresour. Technol. *325*, 124653. https://doi.org/10.1016/j.biortech.2020.124653.
7. Ye, J.W., Lin, Y.N., Yi, X.Q., Yu, Z.X., Liu, X., and Chen, G.Q. (2023). Synthetic biology of extremophiles: a new wave of biomanufacturing. Trends Biotechnol. *41*, 342–357. https://doi.org/10.1016/j.tibtech.2022.11.010.
8. Edbeib, M.F., Wahab, R.A., and Huyop, F. (2016). Halophiles: biology, adaptation, and their role in decontamination of hypersaline environments. World J. Microbiol. Biotechnol. *32*, 135. https://doi.org/10.1007/s11274-016-2081-9.
9. Qiu, J., Han, R., and Wang, C. (2021). Microbial halophilic lipases: A review. J. Basic Microbiol. *61*, 594–602. https://doi.org/10.1002/jobm.202100107.
10. Amoozegar, M.A., Safarpour, A., Noghabi, K.A., Bakhtiary, T., and Ventosa, A. (2019). Halophiles and Their Vast Potential in Biofuel Production. Front. Microbiol. *10*, 1895. https://doi.org/10.3389/fmicb.2019.01895.
11. Xu, T., Mitra, R., Tan, D., Li, Z., Zhou, C., Chen, T., Xie, Z., and Han, J. (2024). Utilization of gene manipulation system for advancing the biotechnological potential of halophiles: A review. Biotechnol. Adv. *70*, 108302. https://doi.org/10.1016/j.biotechadv.2023.108302.
12. Yin, J., Chen, J.C., Wu, Q., and Chen, G.Q. (2015). Halophiles, coming stars for industrial biotechnology. Biotechnol. Adv. *33*, 1433–1442. https://doi.org/10.1016/j.biotechadv.2014.10.008.
13. Srivastava, A.K., Srivastava, R., Sharma, A., Bharati, A.P., Yadav, J., Singh, A.K., Tiwari, P.K., Srivatava, A.K., Chakdar, H., Kashyap, P.L., and Saxena, A.K. (2022). Transcriptome Analysis to Understand Salt Stress Regulation Mechanism of Chromohalobacter salexigens ANJ207. Front. Microbiol. *13*, 909276. https://doi.org/10.3389/fmicb.2022.909276.
14. Onishi, H., and Kushner, D.J. (1966). Mechanism of dissolution of envelopes of the extreme halophile Halobacterium cutirubrum. J. Bacteriol. *91*, 646–652. https://doi.org/10.1128/jb.91.2.646-652.1966.
15. Gunde-Cimerman, N., Plemenitaš, A., and Oren, A. (2018). Strategies of adaptation of microorganisms of the three domains of life to high salt concentrations. FEMS Microbiol. Rev. *42*, 353–375. https://doi.org/10.1093/femsre/fuy009.
16. Li, P.S., Kong, W.L., and Wu, X.Q. (2021). Salt Tolerance Mechanism of the Rhizosphere Bacterium JZ-GX1 and Its Effects on Tomato Seed Germination and Seedling Growth. Front. Microbiol. *12*, 657238. https://doi.org/10.3389/fmicb.2021.657238.
17. Ventosa, A., Nieto, J.J., and Oren, A. (1998). Biology of moderately halophilic aerobic bacteria. Microbiol. Mol. Biol. Rev. *62*, 504–544. https://doi.org/10.1128/mmbr.62.2.504-544.1998.
18. Csonka, L.N., and Hanson, A.D. (1991). Prokaryotic osmoregulation: genetics and physiology. Annu. Rev. Microbiol. *45*, 569–606. https://doi.org/10.1146/annurev.mi.45.100191.003033.
19. Norberg, P., Kaplan, J.G., and Kushner, D.J. (1973). Kinetics and regulation of the salt-dependent aspartate transcarbamylase of Halobacterium cutirubrum. J. Bacteriol. *113*, 680–686. https://doi.org/10.1128/jb.113.2.680-686.1973.
20. Arakawa, T., Yamaguchi, R., Tokunaga, H., and Tokunaga, M. (2017). Unique Features of Halophilic Proteins. Curr. Protein Pept. Sci. *18*, 65–71. https://doi.org/10.2174/1389203717666160617111140.
21. Dym, O., Mevarech, M., and Sussman, J.L. (1995). Structural features that stabilize halophilic malate dehydrogenase from an archaebacterium. Science *267*, 1344–1346. https://doi.org/10.1126/science.267.5202.1344.
22. Xia, Y.L., Sun, J.H., Ai, S.M., Li, Y., Du, X., Sang, P., Yang, L.Q., Fu, Y.X., and Liu, S.Q. (2018). Insights into the role of electrostatics in temperature adaptation: a comparative study of psychrophilic, mesophilic, and thermophilic subtilisin-like serine proteases. RSC Adv. *8*, 29698–29713. https://doi.org/10.1039/c8ra05845h.
23. Kennedy, S.P., Ng, W.V., Salzberg, S.L., Hood, L., and DasSarma, S. (2001). Understanding the adaptation of Halobacterium species NRC-1 to its extreme environment through computational analysis of its genome sequence. Genome Res. *11*, 1641–1650. https://doi.org/10.1101/gr.190201.
24. Wang, T.N., Guan, Q.T., Pain, A., Kaksonen, A.H., and Hong, P.Y. (2019). Discovering, Characterizing, and Applying Acyl Homoserine Lactone-Quenching Enzymes to Mitigate Microbe-Associated Problems Under Saline Conditions. Front. Microbiol. *10*, 823. https://doi.org/10.3389/fmicb.2019.00823.
25. Mevarech, M., Frolow, F., and Gloss, L.M. (2000). Halophilic enzymes: proteins with a grain of salt. Biophys. Chem. *86*, 155–164. https://doi.org/10.1016/s0301-4622(00)00126-5.
26. Sivakumar, N., Li, N., Tang, J.W., Patel, B.K.C., and Swaminathan, K. (2006). Crystal structure of AmyA lacks acidic surface and provide insights into protein stability at poly-extreme condition. FEBS Lett. *580*, 2646–2652. https://doi.org/10.1016/j.febslet.2006.04.017.
27. Peng, T., Cheng, X., Chen, Y., and Yang, J. (2021). Sulfoxide Reductases and Applications in Biocatalytic Preparation of Chiral Sulfoxides: A Mini-Review. Front. Chem. *9*, 714899. https://doi.org/10.3389/fchem.2021.714899.
28. Drazic, A., and Winter, J. (2014). The physiological role of reversible methionine oxidation. Biochim. Biophys. Acta *1844*, 1367–1382. https://doi.org/10.1016/j.bbapap.2014.01.001.
29. Stadtman, E.R., Moskovitz, J., and Levine, R.L. (2003). Oxidation of methionine residues of proteins: biological consequences. Antioxidants Redox Signal. *5*, 577–582. https://doi.org/10.1089/152308603770310239.
30. Achilli, C., Ciana, A., and Minetti, G. (2015). The discovery of methionine sulfoxide reductase enzymes: An historical account and future perspectives. Biofactors *41*, 135–152. https://doi.org/10.1002/biof.1214.
31. Boschi-Muller, S., Olry, A., Antoine, M., and Branlant, G. (2005). The enzymology and biochemistry of methionine sulfoxide reductases. Biochim. Biophys. Acta *1703*, 231–238. https://doi.org/10.1016/j.bbapap.2004.09.016.
32. Yang, J., Yuan, Z., Zhou, Y., Zhao, J., Yang, M., Cheng, X., Ou, G., and Chen, Y. (2016). Asymmetric reductive resolution of racemic sulfoxides by recombinant methionine sulfoxide reductase from a pseudomonas monteilii strain. J. Mol. Catal. B Enzym. *133*, S588–S592. https://doi.org/10.1016/j.molcatb.2017.02.005.
33. Yang, J., Wen, Y., Peng, L., Chen, Y., Cheng, X., and Chen, Y. (2019). Identification of MsrA homologues for the preparation of (R)-sulfoxides at high substrate concentrations. Org. Biomol. Chem. *17*, 3381–3388. https://doi.org/10.1039/c9ob00384c.
34. Wen, Y., Peng, L., Zhou, Y., Peng, T., Chen, Y., Cheng, X., Chen, Y., and Yang, J. (2020). Discovery and application of methionine sulfoxide reductase B for preparation of (S)-sulfoxides through kinetic resolution. Catal. Commun. *136*, 105908. https://doi.org/10.1016/j.catcom.2019.105908.
35. Peng, T., Tian, J., Zhao, Y., Jiang, X., Cheng, X., Deng, G., Zhang, Q., Wang, Z., Yang, J., and Chen, Y. (2022). Multienzyme Redox System with Cofactor Regeneration for Cyclic Deracemization of Sulfoxides. Angew. Chem., Int. Ed. Engl. *61*, e202209272. https://doi.org/10.1002/anie.202209272.
36. Zhao, Y., Jiang, X., Zhou, S., Tian, J., Yang, P., Chen, Y., Zhang, Q., Xu, X., Chen, Y., and Yang, J. (2023). Kinetic resolution of sulfoxides with high enantioselectivity using a new homologue of methionine sulfoxide reductase B. Org. Biomol. Chem. *21*, 3417–3422. https://doi.org/10.1039/d3ob00402c.
37. Zhang, Q., Pan, B., Yang, P., Tian, J., Zhou, S., Xu, X., Dai, Y., Cheng, X., Chen, Y., and Yang, J. (2024). Engineering of methionine sulfoxide reductase A with simultaneously improved stability and activity for kinetic resolution of chiral sulfoxides. Int. J. Biol. Macromol. *260*, 129540. https://doi.org/10.1016/j.ijbiomac.2024.129540.
38. Anselmi, S., Carvalho, A.T.P., Serrano-Sanchez, A., Ortega-Roldan, J.L., Caswell, J., Omar, I., Perez-Ortiz, G., Barry, S.M., Moody, T.S., and Castagnolo, D. (2023). Discovery and Rational Mutagenesis of Methionine Sulfoxide Reductase Biocatalysts To Expand

the Substrate Scope of the Kinetic Resolution of Chiral Sulfoxides. ACS Catal. *13*, 4742–4751. https://doi.org/10.1021/acscatal.3c00372.

39. Nosek, V., and Míšek, J. (2018). Chemoenzymatic Deracemization of Chiral Sulfoxides. Angew. Chem., Int. Ed. Engl. *57*, 9849–9852. https://doi.org/10.1002/anie.201805858.
40. Bierbaumer, S., Schmermund, L., List, A., Winkler, C.K., Glueck, S.M., and Kroutil, W. (2022). Synthesis of Enantiopure Sulfoxides by Concurrent Photocatalytic Oxidation and Biocatalytic Reduction. Angew. Chem., Int. Ed. Engl. *61*, e202117103. https://doi.org/10.1002/anie.202117103.
41. Achilli, C., Ciana, A., and Minetti, G. (2017). Kinetic resolution of phenyl methyl sulfoxides by mammalian methionine sulfoxide reductase A. Tetrahedron Lett. *58*, 4781–4782. https://doi.org/10.1016/j.tetlet.2017.11.022.
42. Boschi-Muller, S., and Branlant, G. (2014). Methionine sulfoxide reductase: chemistry, substrate binding, recycling process and oxidase activity. Bioorg. Chem. *57*, 222–230. https://doi.org/10.1016/j.bioorg.2014.07.002.
43. Fu, X., Adams, Z., Liu, R., Hepowit, N.L., Wu, Y., Bowmann, C.F., Moskovitz, J., and Maupin-Furlow, J.A. (2017). Methionine Sulfoxide Reductase A (MsrA) and Its Function in Ubiquitin-Like Protein Modification in Archaea. mBio *8*, e01169-17. https://doi.org/10.1128/mBio.01169-17.
44. Jaakkola, S.T., Pfeiffer, F., Ravantti, J.J., Guo, Q., Liu, Y., Chen, X., Ma, H., Yang, C., Oksanen, H.M., and Bamford, D.H. (2016). The complete genome of a viable archaeum isolated from 123-million-year-old rock salt. Environ. Microbiol. *18*, 565–579. https://doi.org/10.1111/1462-2920.13130.
45. Wu, Y., Hu, J., Du, Y., Lu, G., Li, Y., Feng, Y., Chen, L., Tu, Y., Xiang, M., Gui, Y., et al. (2023). Mechanistic Insights into the Halophilic Xylosidase Xylo-1 and Its Role in Xylose Production. J. Agric. Food Chem. *71*, 15375–15387. https://doi.org/10.1021/acs.jafc.3c05045.
46. Bowers, K.J., and Wiegel, J. (2011). Temperature and pH optima of extremely halophilic archaea: a mini-review. Extremophiles *15*, 119–128. https://doi.org/10.1007/s00792-010-0347-y.
47. Peng, L., Wen, Y., Chen, Y., Yuan, Z., Zhou, Y., Cheng, X., Chen, Y., and Yang, J. (2018). Biocatalytic preparation of chiral sulfoxides through asymmetric reductive resolution by methionine sulfoxide reductase A. ChemCatChem *10*, 3284–3290. https://doi.org/10.1002/cctc.201800279.
48. Xu, Z., Cen, Y.K., Zou, S.P., Xue, Y.P., and Zheng, Y.G. (2020). Recent advances in the improvement of enzyme thermostability by structure modification. Crit. Rev. Biotechnol. *40*, 83–98. https://doi.org/10.1080/07388551.2019.1682963.
49. Cohen, F.E., and Sternberg, M.J. (1980). On the prediction of protein structure: The significance of the root-mean-square deviation. J. Mol. Biol. *138*, 321–333. https://doi.org/10.1016/0022-2836(80)90289-2.
50. Ali, S.A., Hassan, M.I., Islam, A., and Ahmad, F. (2014). A review of methods available to estimate solvent-accessible surface areas of soluble proteins in the folded and unfolded states. Curr. Protein Pept. Sci. *15*, 456–476. https://doi.org/10.2174/1389203715666140327114232.
51. Galzitskaya, O.V., and Garbuzynskiy, S.O. (2006). Entropy capacity determines protein folding. Proteins *63*, 144–154. https://doi.org/10.1002/prot.20851.
52. Frolow, F., Harel, M., Sussman, J.L., Mevarech, M., and Shoham, M. (1996). Insights into protein adaptation to a saturated salt environment from the crystal structure of a halophilic 2Fe-2S ferredoxin. Nat. Struct. Biol. *3*, 452–458. https://doi.org/10.1038/nsb0596-452.
53. Ebbinghaus, S., Kim, S.J., Heyden, M., Yu, X., Heugen, U., Gruebele, M., Leitner, D.M., and Havenith, M. (2007). An extended dynamical hydration shell around proteins. Proc. Natl. Acad. Sci. USA *104*, 20749–20752. https://doi.org/10.1073/pnas.0709207104.
54. Halle, B. (2004). Protein hydration dynamics in solution: a critical survey. Philos. Trans. R. Soc. Lond. B Biol. Sci. *359*, 1207–1224. https://doi.org/10.1098/rstb.2004.1499.
55. Okajima, R., Hiraoka, S., and Yamashita, T. (2021). Environmental Effects on Salt Bridge Stability in the Protein-Protein Interface: The Case of Hen Egg-White Lysozyme and Its Antibody, HyHEL-10. J. Phys. Chem. B *125*, 1542–1549. https://doi.org/10.1021/acs.jpcb.0c09248.
56. Bandyopadhyay, A.K., Islam, R.N.U., Mitra, D., Banerjee, S., Yasmeen, S., and Goswami, A. (2019). Insights from the salt bridge analysis of malate dehydrogenase from H. salinarum and E.coli. Bioinformation *15*, 95–103. https://doi.org/10.6026/97320630015095.
57. Van Der Spoel, D., Lindahl, E., Hess, B., Groenhof, G., Mark, A.E., and Berendsen, H.J.C. (2005). GROMACS: Fast, flexible, and free. J. Comput. Chem. *26*, 1701–1718. https://doi.org/10.1002/jcc.20291.
58. Trott, O., and Olson, A.J. (2010). AutoDock Vina: improving the speed and accuracy of docking with a new scoring function, efficient optimization, and multithreading. J. Comput. Chem. *31*, 455–461. https://doi.org/10.1002/jcc.21334.
59. DeLano, W.L. (2002). The PyMOL molecular graphics system. https://www.pymol.org/.
60. Humphrey, W., Dalke, A., and Schulten, K. (1996). VMD: visual molecular dynamics. J. Mol. Graph. *14*, 33. https://doi.org/10.1016/0263-7855(96)00018-5.
61. Wu, P.F., Zhang, Z., Guan, X.L., Li, Y.L., Zeng, J.H., Zhang, J.J., Long, L.H., Hu, Z.L., Wang, F., and Chen, J.G. (2013). A specific and rapid colorimetric method to monitor the activity of methionine sulfoxide reductase A. Enzym. Microb. Technol. *53*, 391–397. https://doi.org/10.1016/j.enzmictec.2013.08.005.

STAR★METHODS

KEY RESOURCES TABLE

REAGENT or RESOURCE	SOURCE	IDENTIFIER
Bacterial and virus strains		
TOP10 Chemically Competent Cell	Beijing Tsingke Biotech Co., Ltd.	Cat: TSC-C12
BL21 Star (DE3) Chemically Competent Cell	Beijing Tsingke Biotech Co., Ltd.	Cat: TSC-E01
Chemicals, peptides, and recombinant proteins		
50XTAE Buffer	Sangon Biotech	Cat: B548101-0500
DNA Marker (250~10000 bp)	Sangon Biotech	Cat: B600022-0050
Coomassie Brilliant Blue Quick stain	Epizyme	Cat:PS111
Omni-EasyTM instant protein loading buffer (denatured, reduced, 5 ×)	Epizyme	Cat:LT101S
Two-color pre-staining protein Marker 10 KDa~250 KDa	Epizyme	Cat: WJ102
Oligonucleotides		
Primer: R168K Forward: GAAGGTCGCGAAGGTCAAAG AGGAGTTCGCCGAG	This paper	N/A
Primer: R168K Reverse: CTCGGCGAACTCCTCTTTG ACCTTCGCGACCTTC	This paper	N/A
Primer: R168F Forward: GAAGGTCGCGAAGGTCTTTG AGGAGTTCGCCGAG	This paper	N/A
Primer: R168F Reverse: GAAGGTCGCGAAGGTCTTTGA GGAGTTCGCCGAG	This paper	N/A
Primer: R168A Forward: CGAAGGTCGCGAAGGTCGCGG AGGAGTTCGCCGAGAAG	This paper	N/A
Primer: R168A Reverse: CTTCTCGGCGAACTCCTCCGCG ACCTTCGCGACCTTCG	This paper	N/A
Primer: R168E Forward: GAAGGTCGCGAAGGTCGAAGA GGAGTTCGCCGAG	This paper	N/A
Primer: R168E Reverse: CTCGGCGAACTCCTCTTCGAC CTTCGCGACCTTC	This paper	N/A
Primer: R168P Forward: GAAGGTCGCGAAGGTCCCGG AGGAGTTCGCCGAGAAG	This paper	N/A
Primer: R168P Reverse: CTTCTCGGCGAACTCCTCCGGG ACCTTCGCGACCTTC	This paper	N/A
Critical commercial assays		
Gel Mini Purification Kit	Zomanbio	Cat: ZP202
Site-directed Mutagenesis Kit	Sangon Biotech	Cat: B639281-0020

(*Continued on next page*)

Continued

REAGENT or RESOURCE	SOURCE	IDENTIFIER
BeyoGold™ His-tag Purification Resin	Beyotime	Cat: P2218
BCA protein concentration assay kit	Beyotime	Cat: P0009
Easy PAGE color rapid gel preparation kit (10%)	Seven Biotech	Cat: SW143-02
Software and algorithms		
Origin 2022	Origin	https://www.originlab.com/2022
GraphPad Prism 9.5.0	Prism	https://www.graphpad-prism.cn/
Lasergene	Lasergene	https://www.dnastar.com/software/lasergene/
Gromacs 2020.6	Spoel et al.[57]	https://manual.gromacs.org/2020.6/download.html
Python 3.9	Python Software Foundation	https://www.python.org/downloads/release/python-390/
VMD version 1.9.3	Humphrey et al.[58]	https://www.ks.uiuc.edu/Research/vmd/
PyMOL	DeLano et al.[59]	https://pymol.org/
Autodock Vina	Trott et al.[60]	https://github.com/ccsb-scripps/AutoDock-Vina

EXPERIMENTAL MODEL AND STUDY PARTICIPANT DETAILS

Microbe strains

E. coli strains TOP10 and BL21 (DE3) were used for molecular cloning and the recombinant expression, respectively. The corresponding competent cells were purchased from Tsingke Biotech Co., Ltd, Beijing, China.

METHODS DETAILS

Recombinant expression and purification of *Hh*MsrA and variants

The gene sequence of MsrA from the halophile *H. hubeiense* strain JI20-1 was obtained from the GenBank database and synthesized by Qingke Biotechnology Co., Ltd. (Chongqing, China). The corresponding DNA fragment was then cloned into the multiple cloning site (MCS) of the pET-28a vector using *Bam*H I and *Xho* I restriction sites to construct the recombinant plasmid. To induce the soluble expression of recombinant enzymes, recombinant plasmids were transformed into *E. coli* BL21 (DE3) cells. Overnight cultures of BL21 (DE3) cells harboring the expression plasmid were diluted at a 1:100 ratio in LB medium and incubated at 37°C until the optical density at 600 nm (OD_{600}) reached 0.6. Protein expression was then induced with 1 mM isopropyl β-D-1-thiogalactopyranoside (IPTG) and the cultures were incubated at 20°C for 18 hours. Cells were harvested by centrifugation at 4000 rpm for 10 min and lysed by sonication. The lysates were centrifuged at 12000 rpm for 15 minutes at 4°C to collect the crude enzymes. Purification of the recombinant *Hh*MsrA and variants was achieved through Ni-NTA affinity chromatography using the His_6-tagged within the proteins. Protein concentration was determined using the bicinchoninic acid (BCA) assay and then converted to micromolar (μM) based on the molecular weight of the protein. The purity of the proteins was assessed by SDS-PAGE gel electrophoresis.

Enzyme activity assays

The enzymatic activities of the *Hh*MsrA and its variants were determined using the dithiothreitol (DTT)-5,5′-dithiobis (2-nitrobenzoic acid) (DTNB) coupled colorimetric assay, as previously reported with modifications.[37,61] The consumption of co-factor DTT was used to represent the enzyme activity. For relative activity assays of pH and temperature profiles, reaction mixtures containing purified enzymes (3 μM), Met-O (3 mM), and DTT (1 mM) were combined in a 500 μL reaction system. After a 45 min reaction under different pH or temperature conditions, 50 μL of mixtures from each well were transferred to a 96-well ELISA plate, and 150 μL of DTNB solution were added to a final concentration of 2 mM. After incubation at 37°C for 15 min, the plate was placed into the microplate reader to measure the absorbance at 405 nm (A_{405}). A blank system without enzyme was used as a control. The decrease in A_{405} was used to describe the relative activities to represent the pH and temperature profiles. For the specific activity assays, the same enzymatic reactions were performed at pH 10.0 and 40°C in the presence of various salts and substrates. The amount of enzyme that consumed 1 μM of DTT per minute was defined as 1 unit (U). For analysis of the reversible effect of salt inhibition, the enzyme was first incubated in 2.0 M of Na_2SO_4 for 45 min and then washed with 3 times via ultrafiltration centrifugation. The recovered enzyme was tested for the activity using method mentioned above. Differential significance analysis was conducted using the t-test method, with a *p*-value of less than 0.05 indicating a significant difference.

Half-life and pH stability analysis

To determine the half-life of *Hh*MsrA-WT and *Hh*MsrA-R168K, the enzymes were first incubated at 30°C for up to 50 h without KCl and 270 h with 1.5 M KCl. Enzyme activity was measured at specific time intervals throughout this period using methods described above. The initial

activity was recorded, and subsequent measurements were taken to determine the remaining activity over time, allowing the calculation of the enzyme's half-life. The data were then fitted using Origin 2022 to calculate the enzyme's half-life. To determine the pH stability, the enzyme was incubated in solutions with pH 5.0, 7.0, and 11.0 for 2 h or 10 h with or without 1.5 M of KCl. Then, enzyme activity was measured using methods described above.

Kinetic parameters determination

To determine the kinetic parameters, 3 μM *Hh*MsrA-WT of was incubated with the substrate Met-O, varying the concentrations from 0.2 to 20 mM (containing 0.1 to 10 mM of the *S* enantiomers) under high salt condition (1.5 M KCl). Additionally, 12 μM of *Hh*MsrA-WT was incubated with the substrate Met-O, varying the concentrations from 0.4 to 30 mM (containing 0.2 to 15 mM of the *S* enantiomers) under low salt condition (0.8 M KCl). For the variants, 3 μM of *Hh*MsrA-R168K and 15 μM of *Hh*MsrA-R168P were incubated with the substrate Met-O, varying the concentrations from 0.2 to 20 mM (containing 0.1 to 10 mM of the *S* enantiomers). The initial rate at different substrate concentrations was determined by the above colorimetric assay after a 20 min incubation at 40°C. K_{cat} and K_m values were calculated using nonlinear regression analysis in software Origin 2022, according to the Michaelis-Menten equation.

Site-directed mutagenesis

Site-directed mutagenesis of *Hh*MsrA was performed via PCR using the Site-Directed Mutagenesis Kit (Sangon Biotech, China). The PCR primers were listed in the key resources table, and the parameters were set as follows: 95°C for 5 min (1 cycle), 95°C for 30 s, 60°C for 30 s, and 68°C for 10 min (30 cycles). The PCR products were then digested with *Dpn* I at 30°C for 3 h to eliminate the template DNA. Subsequently, the products were transformed into *E. coli* BL21 (DE3) cells, and sequencing was conducted to confirm the mutagenesis.

Molecular docking and MD simulations

The 3D models of both the wild-type *Hh*MsrA and its variants were created using the SWISS-MODEL web server, with the *Neisseria meningitidis* Z2491 MsrA crystal structure (PDB ID: 3BQE) as the modeling template (43.71% of sequence identity). The substrate Met-*S*-O was sourced from PubChem. Autodock tools were used to produce PDBQT files for the substrate and protein, which were then docked using Vina in a semiflexible manner. The docking process was repeated three times to ascertain the most favorable binding affinity, selecting the best complex conformation. Visualization was done using PyMOL software. For molecular dynamics (MD) simulations, Gromacs 2022.06 was employed, incorporating protein residues from the AMBER14SB force field and the substrate using the GAFF. The simulations used a periodic cubic box, ensuring a 10 Å buffer from the solute to the box edges, filled with TIP3P water molecules, and balanced with Na^+, K^+, and Cl- ions for neutrality. Energy minimization was conducted via the steepest descent method, followed by NVT (500 ps) and NPT (1,000 ps) equilibration phases, using the linear constraint solver for hydrogen bonds and the particle-mesh Ewald method for long-range interactions, setting a 1.0 nm cutoff for van der Waals forces. MD simulations were carried out at 303 K in 0 or 1 M KCl. The analysis utilized a suite of tools from Gromacs, such as gmx rms, rmsf, gyrate, sasa, and spatial, to evaluate various molecular dynamics parameters: RMSD, RMSF, Rg, SASA, SDF, and the molecular or atomic density distribution within the system. Trajectory analysis and the identification of salt bridges were conducted using Visual Molecular Dynamics (VMD), applying a cutoff for oxygen-nitrogen distances at 4 Å.

QUANTIFICATION AND STATISTICAL ANALYSIS

All statistical analysis was performed with GraphPad Prism 9.5.0. Data were derived from three independent biological replicates reported as mean ± standard deviation ($n = 3$). The t-test or nonparametric test was used for the comparison of two independent samples, with $p < 0.05$ indicating statistical significance (*$p < 0.05$, **$p < 0.01$, ***$p < 0.001$).